"***This is the pre-peer reviewed version of the following article:*** Wagner, S., Auerbach, H., Tait, C. E., Martinaiou, I., Kumar, S. C. N., Kübel, C., Sergeev, I., Wille, H. C., Behrends, J., Wolny, J. A., Schünemann, V., Kramm, U. I. (**2019**). Elucidating the Structural Composition of a Fe – N – C Catalyst by Nuclear- and Electron-Resonance Techniques. *Angew. Chem. Int. Ed.*, 58, 10486-10492, ***which has been published in final form at*** https://doi.org/10.1002/anie.201903753. ***This article may be used for non-commercial purposes in accordance with Wiley Terms and Conditions for Use of Self-Archived Versions."***

Elucidating the structural composition of a Fe-N-C catalyst by nuclear and electron resonance techniques

S. Wagner [a,b], H. Auerbach [c], C.E. Tait [d], I. Martinaiou [a,e], C.N. Shyam Kumar [a,f], C. Kübel [a,f,g], I. Sergeev [h], H.C. Wille [h], J. Behrends [d], J.A. Wolny [c], V. Schünemann [c], U.I. Kramm *, [a, b, e]

Abstract. *Fe-N-C catalysts are very promising materials for fuel cells and metal air batteries. This work gives fundamental insights into the structural composition of a Fe-N-C catalyst and highlights the importance of an in-depth characterization. By nuclear- and electron-resonance techniques, we are able to show that even after mild pyrolysis and acid leaching the catalyst contains considerable fractions of alpha iron and surprisingly iron oxide. Our work makes it questionable to what extent indeed FeN_4 sites can be present in Fe-N-C catalysts prepared by pyrolysis at 900 °C and above. The simulation of the iron partial density of phonon states enables identification of three FeN_4 species in our catalyst, one of them comprising a sixfold coordination with end-on bonded oxygen as one of the axial ligands.*

Non-precious metal catalysts of Fe-N-C type play an important role as possible catalyst material in proton exchange fuel cells (PEFC), alkaline fuel cells (AFC) and metal air batteries [1].

It is known that for the preparation of these catalysts iron, nitrogen and carbon are required during a high temperature pyrolysis. When using independent Fe and N precursors, the pyrolysis needs to be performed at temperatures exceeding 600 °C, but the optimum temperature strongly depends on the selected precursors. Molecular FeN_4 centers were identified by different groups as ORR active sites [2]. In this respect, especially Mössbauer spectroscopy is very powerful [3]:

[a] TU Darmstadt, Graduate School Energy Science and Engineering, Otto-Berndt-Str. 3, 64287 Darmstadt, Germany

[b] TU Darmstadt, Department of Material and Earth Sciences, Otto-Berndt-Str. 3, 64287 Darmstadt, Germany

[c] TU Kaiserslautern, Department of Physics, Biophysics and Medical Physics, Erwin-Schrödinger-Strasse 46, 67663 Kaiserslautern, Germany

[d] Freie Universität Berlin, EPR spectroscopy in photovoltaics, Arnimallee 14, 14195 Berlin, Germany

[e] TU Darmstadt, Department of Chemistry, Otto-Berndt-Str. 3, 64287 Darmstadt, Germany

[f] Karlsruhe Institute of Technology (KIT), Institute for Nanotechnology, Campus North, Hermann-von-Helmholtz-Platz 1, 76344 Eggenstein-Leopoldshafen, Germany

[g] Karlsruhe Institute of Technology (KIT), Nano Micro Facility, Campus North, Hermann-von-Helmholtz-Platz 1, 76344 Eggenstein-Leopoldshafen, Germany

[h] Deutsches Elektronen-Synchrotron, Notkestraße 85, 22607 Hamburg, Germany

* corresponding author email address: kramm@ese.tu-darmstadt.de

Changes in the local environment of FeN_4 sites, e.g. by axial binding of reaction intermediate, will lead to well pronounced changes in the isomer shift (δ, as related to electron density) and quadrupole splitting (ΔE_Q, as related to the electric field gradient at the nucleus). Thus, especially in porphyrin and heme chemistry it is a widely used technique. For the investigation of Fe-N-C catalysts, the materials so far assigned as purest contained only two, respectively three doublets overlaying in their Mössbauer spectra [2c, 2d].

It is important to note, that these catalysts were obtained by very different approaches, but two of the identified iron sites were the same, named D1 and D2.

For the so-called D1 doublet (δ = 0.3 mm s^{-1}, ΔE_Q = 0.9 mm s^{-1}) a direct correlation between the iron content related to this site and the ORR activity in terms of kinetic current density was found by Koslowski et al. [2a]. Based on additional data for their system, the D1 site was assigned to a ferrous low spin iron in a N_4 environment [2a, 4]. However, similar Mössbauer parameters as for the D1 doublet can be found for iron oxide nanoparticles in RT Mössbauer spectroscopy. Due to the acid-leaching treatment of all of our catalysts, iron oxide species were excluded so far, as they are not stable in acidic conditions. Nevertheless, the oxidation state and structure under reaction conditions remains under debate, but both are crucial for basic understanding the reaction mechanism active in Fe-N-C catalysts.

While today's most active Fe-N-C catalysts are prepared from metal organic frameworks (MOFs) such as zinc imidazole frameworks (ZIFs) or polyaniline in combination with an iron source and possibly a secondary nitrogen precursor [1b, 5], pyrolyzed carbon supported iron porphyrins and phthalocyanines are very good model systems. Due to the initial presence of FeN_4 coordination, ORR active materials are formed even at low pyrolysis temperatures such as 600 °C [4, 6]. As illustrated in our recent research news [3] for such low pyrolysis temperatures the contribution of inorganic iron species such as elemental iron or iron carbide can be neglected.

RT ^{57}Fe Mössbauer spectroscopy is successfully used by different groups to investigate the oxidation states and chemical environment of Fe-N-C catalyst [4, 7]. In order to gain additional insight to the iron sites and the hyperfine interaction, low temperature Mössbauer spectroscopy can be used. Cooling the sample to

several Kelvin give rise to magnetic splitting due to the reduced spin relaxation with a spectral shape that crucially depends on the behavior of the electronic wave functions which can be determined by the Spin Hamiltonian [8]. Therefore, LT Mössbauer spectroscopy is widely used as characterization technique for iron containing biomolecules and heme like proteins [9]. With respect to Fe-N-C catalysts, Sougrati et al. performed a temperature-dependent study to determine Lamb-Mössbauer factors [10]. In addition, the measurements at 5 K showed that the so-called D1 doublet is an overlay of FeN_4 sites and iron oxide nanoparticles in their catalyst. Based on the synthesis route of their catalysts, the presence of oxidic species was not unexpected for us, as the catalyst was prepared from ZIF-8, iron acetate and phenanthroline by a high-temperature pyrolysis (> 900 °C) without acid leaching. Thus, even working at low iron loadings makes it likely, that not all the iron remains in an intact N_4-environment, but oxidic species might be formed after contact with air.

Kneebone et al. [7b] used Mössbauer spectroscopy at 80 K and Nuclear Inelastic Scattering (NIS) to characterize a PANI-based Fe-N-C catalyst. NIS is a nuclear resonant technique that uses the annihilation of phonons by the absorption of an incident X-ray from a synchrotron beam. Complementary to Mössbauer spectroscopy where the recoil free resonance is used, NIS uses the inelastic sidebands in the energy spectrum around the elastic peak which than yields the iron partial density of phonon states (pDOS). Further it reveals the full spectrum of vibrational dynamics of the probed Mössbauer nuclei and allows the identification of modes which are not available by other techniques [11]. DFT calculations modulate the partial iron density of phonon states (pDOS) [12]. Kneebone et al. suggested, based on their NIS data and Mössbauer spectra in combination with DFT calculations, that edge-hosted sites of FeN_4-type or Fe_2N_5-type are responsible for oxygen and NO binding for their catalyst. Due to the strong inhomogeneity of their catalyst, further clear conclusions were not possible.

Herein, we present a detailed structural characterization of a Fe-N-C model catalyst by Mössbauer spectroscopy at different temperatures in combination with NIS and X-band Electron Paramagnetic Resonance spectroscopy (EPR). The catalyst was prepared from carbon-supported chloro-iron tetramethoxyphenyl-porphyrin (FeTMPPCl). The preparation conditions were selected in a way to ensure exclusive presence of FeN_4 sites based on our previous pyrolysis-temperature dependent study [4]: Thus, the catalyst is prepared with low iron loading, low pyrolysis temperature (600 °C) and acid-leaching (1M HCl overnight).

In Figure 1a measurements with the rotating disc electrode (RDE) are shown that confirm the relatively good performance of our catalyst. An onset potential of U_{onset} = 0.790 V, a half-wave potential of $U_{1/2}$ = 0.668 V vs. RHE and a diffusion limiting current density of $I_{diff\ lim}$ = -5.7 mA cm^{-2} are found. A kinetic current density at 0.75 V of 0.6 mA cm^{-2} can be calculated. The catalyst shows characteristics which are well known for porphyrin-based catalysts [13].

First, we would like to discuss the structural composition of the catalyst as derived by Mössbauer spectroscopy at RT (Fig. 1b), scanning transmission electron microscopy (STEM) (Fig. 1c) and EPR spectroscopy at 5 K (Fig. 1d). The Mössbauer spectrum looks very similar to other porphyrin-based catalysts prepared at low pyrolysis temperature [2c, 6, 14]. It was fitted with three

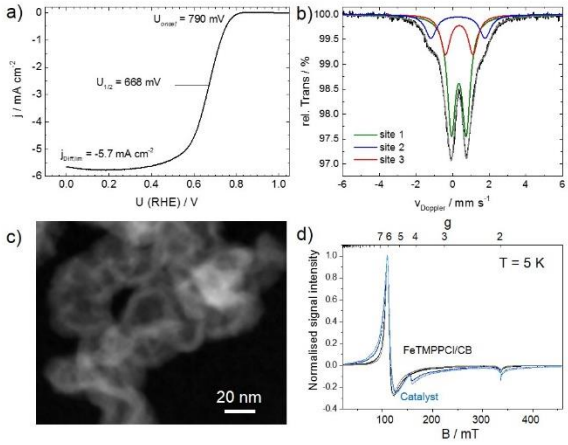

Figure 1. a) RDE measurement of our catalyst in 0.1M H_2SO_4, b) room temperature Mössbauer spectrum, c) STEM image and d) X-band EPR spectrum of the catalyst (5 K). For reasons of comparison the FeTMPPCl/CB precursor spectrum is added in d).

Table 1. Mössbauer parameters of the RT-Mössbauer spectrum. Calibration was made versus alpha iron at RT.

Component	site 1	site 2	site 3
Assignment	D1 site	FePc-like	heme-like
δ / mm s^{-1}	0.34	0.29	0.36
ΔE_Q /mm s^{-1}	0.81	2.96	1.50
Γ / mm s^{-1}	0.54	0.72	0.62
Area† / %	59.4	16.9	23.7

iron sites, all assigned to doublet species. In this work, we would like to label the doublets as site 1 (D1), site 2 (D2) and site 3 (D3), the color code is the same as in previous work [2a, 2d, 15]. The Mössbauer parameters as well as the relative absorption areas are summarized in Table 1.

The assignment of iron species to these sites will be discussed later. (S)TEM images (Figure 1c and S1) are in line with the interpretation that under such mild preparation conditions the catalyst gives no indication of iron or iron oxide nanoparticle formation. Only a well dispersed Fe-rich shell, formed by the carbonization of iron porphyrin, is found. A line profile over the carbon areas of lower and higher density (see insert in Figure S1) also confirms the absence of iron and iron oxide particles.

In Figure 1d the X-band EPR spectrum of the catalyst is compared to the spectrum of the carbon-supported porphyrin (FeTMPPCl/CB) that was used as precursor. For reasons of comparison, the signal intensity was normalized. FeTMPPCl/CB gives an EPR signal as expected for a square pyramidal ferric high spin FeN_4 site with chlorine as axial ligand with effective g-values of 6.0 and 2.0 [16]. The EPR spectrum of the catalyst shows the same high spin Fe(III) signal, but it is broadened compared to the precursor signal, indicating the presence of a heterogeneous distribution of iron in the sample. An additional minor contribution at g_{eff} = 4.3 is found for our catalyst. It might be due to oxidized iron or a minor contributing FeN_4 or other impurity species [17]. Quantitation of the ferric iron content in the catalyst was performed by using FeTMPPCl/CB with known Fe(III) content as a reference. In order to accurately determine the contribution of high spin Fe(III) and exclude errors due to the presence of additional impurity signals and background contributions, the spin

concentration was determined from the double integral of the simulated catalyst spectrum. Values between 20 – 40 % of the overall iron content were obtained for three independent sample measurements (Figure S2, Table S1-S2). The values are slightly larger than estimated from RT Mössbauer spectroscopy. Kramm et al. [18] estimated about 11 % ferric spin state species for a similar catalyst but with lower iron content.

Figure 2a shows the iron partial density of phonon states (pDOS), as derived from the NIS measurements. Figure 2b and c give the comparison of the measurement data with two fit models that will be discussed, later. The typical wavenumber ranges for Fe-N_{pyr}, Fe-N_{His} and vibrations related to oxygen coordination on FeN_4 sites are indicated. There is a surprisingly large background that is untypical for FeN_4-type iron environments. A comparison to literature shows a reasonably good agreement with iron oxide clusters and possibly iron clusters [19]. The number of agglomerated iron atoms in both of these iron sites must be very small, considering the STEM images and Mössbauer spectra obtained at low temperature and as given in Figure 3.

First, let us analyze the pDOS data qualitatively with respect to FeN_4 species: Scheidt et al. [11a] differentiate three main vibrational mode categories for heme samples. The frequency modes from 400 cm^{-1} to 600 cm^{-1}, typically involving iron- and the axial ligand vibrational modes, the mid-range modes (200 cm^{-1} to 400 cm^{-1}) primarily assigned as in-plane modes, and modes below about 200 cm^{-1} mainly containing out-of-plane modes. Zeng et al. [20] related the vibration modes between 120 cm^{-1} to 230 cm^{-1} as Fe-N_{His}. The modes between 250 cm^{-1} to 380 cm^{-1} are assigned to Fe-N_{pyr}. A very dominant feature around 381 cm^{-1} and 395 cm^{-1} can be seen which was not found by Kneebone et al. [7b] for their PANI-based catalyst in any of the

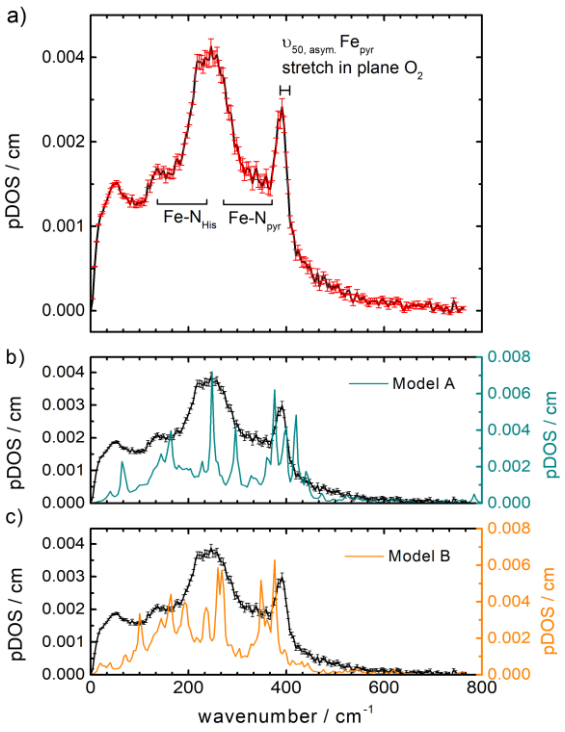

Figure 2. a) Calculated iron pDOS spectrum with specific vibration modes as addressed in the text. b) Model A - Fit of the iron pDOS based on the simulated spectra of iron oxide clusters and iron sites as plotted in Figure 4 a-c and c) Model B - Fit of the iron pDOS based on the simulated spectra of iron oxide clusters and iron sites as plotted in Figure 4 a, b and d.

investigated states (reduced or NO-treated). The position of this most intensive peak (400 cm^{-1}) seems to be in-line with a vibration of a heme-type FeN_4 center interacting with an end-on bonded oxygen molecule (that means in total sixfold coordinated) [21]. According to Rai et al. [22] it is an in-plane, asymmetric stretching mode. Indeed, we believe that this vibration shows the attachment of molecular oxygen to the FeN_4 site. Due to the storage in air, the active sites should already be oxygenated without applying any potential.

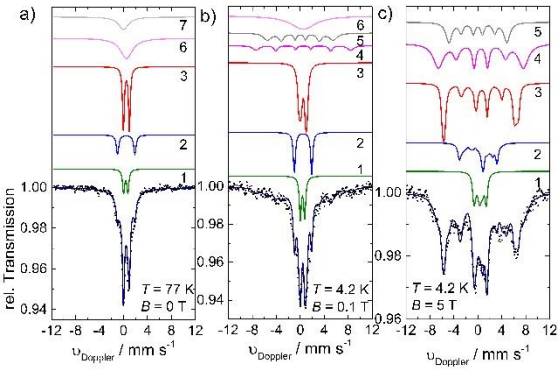

Figure 3. Mössbauer spectra obtained at a) 77 K, B = 0 T, b) 4.2 K with B = 0.1 T and c) 4.2 K with B = 5 T. The Mössbauer parameters are listed in Table 2.

Table 2. Mössbauer parameters as obtained from the analysis of the Mössbauer spectra of the catalyst displayed in Figure 3, absorption areas are given for the spectrum obtained at 4.2 K, 0.1 T. All simulations shown in Figure 3 have been analyzed with one consistent data set, except some different values in linewidths Γ, line ratio I_1:I_2:I_3, area and hyperfine field B_{hf} are given in the corresponding footnotes.

Comp.	1	2	3	4	5	6	7
	Fe(II) LS	FePc	Heme	Particles Fe-O	Particles α-Fe	Part. Fe-O relax	Part. α-Fe relax
S	0	1	$^5/_2$[$]	-	-	-	-
δ / mm s^{-1}	0.37	0.46	0.48	0.50	0.00	0.50	0.00
ΔE_Q / mm s^{-1}	0.72	2.90	1.00	-	-	0.00	0.00
η	0.5	1.0	0.0	-	-	-	-
B_{hf} [+] / T	-	-	-	49.0	34.0	-	-
Γ[§] / mm s^{-1}	0.40	0.42	0.50	0.50;0.70;1.20	0.60;1.00;1.60	5.00	-
I_1:I_2:I_3[#]	-	-	-	3.0:2.0:1.0	3.0:2.0:1.0	-	-
D / cm^{-1}	-	8 ± 1	5 ± 1	-	-	-	-
E/D	-	0.33	0.005	-	-	-	-
β / °	-	43	32	-		-	-
$A_{xx,yy,zz}/\mu_N g_N$ / T	-	-22.0 ± 1; -22.0 ± 1; -22.0 ± 1;	-20.0 ± 0.5; -18.0 ± 0.5; -20.0 ± 0.5;	-	-	-	-
Area[†] / %	12.0 ± 2	12.0 ± 2	28.0 ± 1	8.0 ± 1	16.0 ± 1	24.0 ± 2	0.0

[$] The spin-Hamilton simulations of comp. 3 at T = 77 K in Figure 3a were performed with an external field of B = 44 µT orthogonal to the γ-ray, which corresponds to the strongest part of the earth's magnetic field in Kaiserslautern, Germany.

[+] B_{hf} at 4.2 K and 5 T for comp. 4: 44.0 T and for comp. 5: 30.0 T.

[§] Γ at 77 K in Figure 3a for comp. 3: 0.35 mm s^{-1}; comp. 3: 0.48 mm s^{-1}; comp. 6: 2.50 mm s^{-1}; comp. 7: 2.00 mm s^{-1}. Γ at 4.2 K and 5 T in Figure 3c for comp. 1: 0.50 mm s^{-1}; comp. 2: 0.45 mm s^{-1}; comp. 2: 0.50 mm s^{-1}; comp. 4: $\Gamma_{1,2,3}$ = (0.70 mms^{-1}, 1.20 mm s^{-1}, 2.00 mm s^{-1}); comp. 5: $\Gamma_{1,2,3}$ = (0.70 mms^{-1}, 0.80 mms^{-1}, 1.20 mm s^{-1}).

[#] I_1:I_2:I_3 for comp. 4 and comp. 5 at 4.2 K and 5 T: (3.0:1.0:1.0).

[†] Area at 77 K in Figure 3a for comp. 4: 0 %; for comp. 5: 0 %; comp. 6: 32.0 ± 1 %; comp. 7: 16.0 ± 1 %. Area at 4.2 K and 5 T in Figure 3c for comp. 4: 32.0 ± 1%; comp. 5: 16.0 ± 1 %; comp. 6: 0 %.

It is clear from the heterogeneous and amorphous character of the catalyst that an unambiguous assignment is hard just by comparison to the RT Mössbauer spectroscopy data. Therefore, we would like to discuss the Mössbauer spectra obtained at low temperature.

The picture of iron phases in our catalyst changes when the low-temperature Mössbauer spectra as given in Figure 3 are considered: By cooling down the sample to 77 K (Figure 3a) already two more species can be identified which were not visible during the RT Mössbauer measurement. Unexpectedly, these sites can be attributed to alpha iron and iron oxide. Their relaxed appearance underlines their missing magnetic order. Based on this, we assume very small iron clusters of only a distinct number of atoms. If the relaxation time of small domain structures is smaller than the time window of the measurement, the random domain switching smears the magnetic behavior and the Mössbauer signature collapses to a doublet or singlet [2a, 5e, 7d, 23].

By decreasing the sample temperature, the lifetime of excited states becomes longer and can help to enable magnetic ordering. Comparing the Mössbauer spectra in Figure 3 with the RT measurement in Figure 1b, it becomes clear that a temperature of 4.2 K with 0.1 T is required to stabilize magnetic ordering of alpha iron clusters. Even at this condition, a partial fraction of iron oxide clusters remain in the relaxed state. Only applying an external magnetic field of 5 T was sufficient to enable magnetic ordering for these clusters (Figure 3c). This is different to the $Fe_{0.5d}$ catalyst investigated by Sougrati et al.[10] There, cooling to 5 K was sufficient for magnetic ordering, indicating larger sizes of the iron oxide phases. Details of the LT Mössbauer fitting procedure are described in the Supporting Information. Based on it the Mössbauer parameters as summarized in Table 2 were obtained.

While the absorption areas of sites 2 and 3 are in good agreement with the values obtained from the RT Mössbauer spectrum, the area related to site 1 becomes dramatically decreased. After cooling to 4.2 K, it becomes clear, that only 12 % of the overall iron can be attributed to a ferrous low-spin site, previously assigned as D1 (or here site 1 measured at room temperature). Thus, based on the low-temperature Mössbauer spectra it becomes clear, that even with the mild preparation parameters (in comparison to several other Fe-N-C catalysts) used in this work, the catalyst contains about 50 % of inorganic iron species. Due to the performed acid leaching, especially the presence of oxide clusters was rather unexpected. As the precursor consists of a carbon black and FeTMPPCl, the oxygen content in the precursor was rather low. Based on this, oxide cluster formation must have taken place after the pyrolysis either during the acid leaching or later. As no oxidative dissolution is visible in the cyclic voltammetry in nitrogen saturated electrolyte (Figure S3), these clusters do not seem to be accessible to the electrolyte. In contrast, it is likely, that the alpha iron clusters are indeed embedded in carbon. Thus, for the fitting of our pDOS data (Figure 2a) in principle also iron oxide clusters as found by Marx et al. [19b] or small iron nanoparticles and layers [19a, 24] should be considered. For the LT Mössbauer spectra the content of ferric FeN_4 is even better in agreement with the EPR data compared to the RT Mössbauer data. Approximately, 30 % are assigned to the ferric state. Thus, the contribution is the largest among the FeN_4-type sites.

Having a more distinct knowledge on the iron sites contributing to our spectrum, our NIS data were analyzed more quantitatively by comparison to literature data [9c, 11a, 19, 22, 24-25] combined with DFT calculations. Two models A and B were obtained based on the Mössbauer parameters provided in Table 2. These are already plotted in Figure 2b and c, a complete fitting of the pDOS cannot be obtained but some important characteristic features can be projected by DFT calculations.

The assumed FeN_4 structures implemented in the modeling of the iron pDOS spectrum are shown in Figure 4. Considering the ferrous low spin FeN_4 site: The typical coordination for such complex is sixfold [3]. Furthermore, in related to Zitolo et al. and Li et al. [2d, 2e] the presence of oxygen as one axial ligand seems likely. Based on this the ferrous low-spin site was modulated with oxygen as one axial ligand and a nitrogen as sixth ligand (Figure 4a). For site 2 the Mössbauer parameters are close to FePc, therefore this structural motif was considered in the calculations (Figure 4b). The ferric FeN_4 site is most likely fivefold coordinated. Here, two different possibilities were considered: the initial porphyrin structure with chlorine as axial ligand (Figure 4c) and as an alternative a FeN_4 site with nitrogen as axial ligand (Figure 4d). Related to the porphyrin-type structure, thermogravimetry coupled with mass spectrometry indicated that at 600 °C only 50 – 70 % of the chlorine ligand were released [18]. Based on that it would be possible that to some extent this porphyrin-type coordination still remains intact.

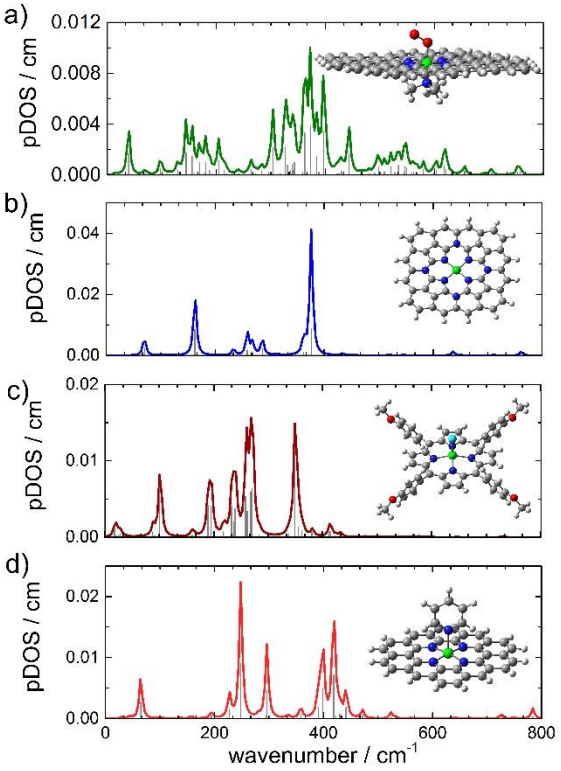

Figure 4. Simulated iron pDOS of (a) $Fe^{2+}N_4$ with trimethylamine and O_2 as axial ligands (low spin) (b) iron phthalocyanine-type coordination embedded in carbon (mid spin) (c) FeTMPPCl, i.e. ferric FeN_4 sites with chlorine as axial ligand (high spin) and (d) ferric FeN_4 site with an axial pyridine ligand. (Color code: grey: carbon, white: hydrogen, blue: nitrogen, green: iron, cyan: chlorine, red: oxygen.)

Model A (Figure 2b) is the sum of the iron partial pDOS spectra for Fe(II) LS (Figure 4a), the FePc like component (Figure 4b), the heme-like iron porphyrin structure of the precursor (Figure 4c) and iron oxide nanoparticles (taken from Marx et al. [19b]), for each species the relative amounts as found by LT Mössbauer spectroscopy were considered. For **Model B** (Figure 2c) the catalyst was simulated with the same species as mentioned above, except that instead of the porphyrin structure, a ferric high-spin FeN_4 site was used with pyridine as axial ligand (Figure 4d). Due to the heterogeneous character of Fe-N-C catalyst the huge size distribution of different kind of particles, as seen from the LT Mössbauer spectroscopy data, makes it very hard to represent the overall NIS spectra. Thus, even those iron clusters will contribute to the pDOS of our catalyst, they were not considered due to the different size effects of NPs [19a].

There are important conclusions to be made: Even under very mild preparation conditions and a subsequent acid leaching Fe-N-C catalysts contain considerable fractions of inorganic clusters (iron and iron oxides). Beside these inorganic species, by NIS we found very strong evidence for a sixfold coordinated heme-type FeN_4 site with an end-on binding oxygen molecule that most probably is at the origin of the ORR activity. However, the large contribution of inorganic iron species to the D1 doublet identified at RT Mössbauer spectroscopy underlines the importance of low-temperature measurements or more advanced characterization methods. Nevertheless, these conclusions are of great importance for further improvement of Fe-N-C preparation strategies as well for a fundamental understanding of the reaction mechanism related to the oxygen reduction in either fuel cells or metal air batteries.

Experimental part.

The experimental section is implemented in the Supporting Information

Acknowledgement.

The NIS experiments were performed at the P01 beamline (Petra III, DESY) as part of the proposal I-20160285. The possibility to perform these experiments is gratefully acknowledged. Financial support via the BMBF joint project contract No 05K16RD1 (UIK + SW) and the DFG project GSC1070 (UIK + IM) is acknowledged. CET would like to acknowledge financial support through a Marie Curie Individual Fellowship (H2020-MSCA-IF-743419).

Keywords. non-precious metal catalysts • oxygen reduction reaction • spectroscopy • energy conversion • Fe-N-C catalyst

References.

[1] a) Z. L. Wang, D. Xu, J. J. Xu, X. B. Zhang, *Chem Soc Rev* **2014**, *43*, 7746-7786; b) F. Jaouen, E. Proietti, M. Lefèvre, R. Chenitz, J.-P. Dodelet, G. Wu, H. T. Chung, C. M. Johnston, P. Zelenay, *Energy Environ. Sci.* **2011**, *4*, 114-130; c) X. Zhao, M. Chen, J. Zuo, J. Wang, Z. Liu, L. Wang, B. Liu, G. Wu, H. Zhang, H. Yang, *Journal of The Electrochemical Society* **2018**, *165*, F1278-F1285.

[2] a) U. I. Koslowski, I. Abs-Wurmbach, S. Fiechter, P. Bogdanoff, *J. Phys. Chem. C* **2008**, *112*, 15356–15366; b) U. I. Kramm, M. Lefèvre, N. Larouche, D. Schmeisser, J.-P. Dodelet, *J. Am. Chem. Soc.* **2014**, *136*, 978−985; c) U. I. Kramm, I. Herrmann-Geppert, J. Behrends, K. Lips, S. Fiechter, P. Bogdanoff, *J. Am. Chem. Soc.* **2016**, *138*, 635−640; d) A. Zitolo, V. Goellner, V. Armel, M. T. Sougrati, T. Mineva, L. Stievano, E. Fonda, F. Jaouen, *Nature Materials* **2015**, *14*, 937-942; e) J. Li, S. Ghoshal, W. Liang, M.-T. Sougrati, F. Jaouen, B. Halevi, S. McKinney, G. McCool, C. Ma, X. Yuan, Z.-F. Ma, S. Mukerjee, Q. Jia, *Energy Environ. Sci.* **2016**, *9*.

[3] U. I. Kramm, L. Ni, S. Wagner, in *Advanced Materials* **2019,** DOI: 10.1002/adma.201805623.

[4] U. I. Kramm, I. Abs-Wurmbach, I. Herrmann-Geppert, J. Radnik, S. Fiechter, P. Bogdanoff, *Journal of The Electrochemical Society* **2011**, *158*, B69-B78.

[5] a) E. Proietti, F. Jaouen, M. Lefevre, N. Larouche, J. Tian, J. Herranz, J. P. Dodelet, *Nature Communications* **2011**, *2:416*; b) Z. Liu, F. Sun, L. Gu, G. Chen, T. Shang, J. Liu, Z. Le, X. Li, H. B. Wu, Y. Lu, *Advanced Energy Materials* **2017**, *7*, 1701154; c) R. Wu, J. Wang, K. Chen, S. Chen, J. Li, Q. Wang, Y. Nie, Y. Song, H. Chen, Z. Wei, *Electrochimica Acta* **2017**, *244*, 47-53; d) N. D. Leonard, S. Wagner, F. Luo, J. Steinberg, W. Ju, N. Weidler, H. Wang, U. I. Kramm, P. Strasser, *ACS Catalysis* **2018**, 1640-1647; e) M. Ferrandon, A. J. Kropf, D. J. Myers, K. Artyushkova, U. Kramm, P. Bogdanoff, G. Wu, C. M. Johnston, P. Zelenay, *The Journal of Physical Chemistry C* **2012**, *116*, 16001-16013.

[6] A. L. Bouwkamp-Wijnoltz, W. Visscher, J. A. R. v. Veen, E. Boellaard, A. M. v. d. Kraan, S. C. Tang, *J. Phys. Chem. B* **2002**, *106*, 12993-13001.

[7] a) A. Morozan, M. T. Sougrati, V. Goellner, D. Jones, L. Stievano, F. Jaouen, *Electrochimica Acta* **2014**, *119*, 192-205; b) J. L. Kneebone, S. L. Daifuku, J. A. Kehl, G. Wu, H. T. Chung, M. Y. Hu, E. E. Alp, K. L. More, P. Zelenay, E. F. Holby, M. L. Neidig, *The Journal of Physical Chemistry C* **2017**, *121*, 16283-16290; c) S. Wagner, I. Martinaiou, A. Shahraei, N. Weidler, U. I. Kramm, *Hyperfine Interact* **2018**, *239:10*; d) H. Schulenburg, S. Stankov, V. Schünemann, J. Radnik, I. Dorbandt, S. Fiechter, P. Bogdanoff, H. Tributsch, *J. Phys. Chem. B* **2003**, *107*, 9034-9041.

[8] H. H. Wickman, M. P. Klein, D. A. Shirley, *Physical Review* **1966**, *152*.

[9] a) E. Bill, V. Schünemann, A. X. Trautwein, R. Weiss, J. Fischer, A. Tabard, R. Guilard, *Inorganica Chimica Acta* **2002**, *420*, 420-426; b) V. Mereacre, M. Schlageter, A. Eichhöfer, T. Bauer, J. A. Wolny, V. Schünemann, A. K. Powell, *Journal of Magnetism and Magnetic Materials* **2016**, *407*, 87-91; c) J. Li, B. C. Noll, A. G. Oliver, C. E. Schulz, W. R. Scheidt, *J. Am. Chem. Soc.* **2013**, *135*, 15627-15641.

[10] M. T. Sougrati, V. Goellner, A. K. Schuppert, L. Stievano, F. Jaouen, *Catalysis Today* **2016**, *262*, 110-120.

[11] a) W. R. Scheidt, J. Li, J. T. Sage, *Chem Rev* **2017**, *117*, 12532-12563; b) H. Auerbach, I. Faus, S. Rackwitz, J. A. Wolny, F. A. Walker, A. I. Chumakov, H. Ogata, M. Knipp, V. Schünemann, *Hyperfine Interactions* **2013**, *226*, 439-443.

[12] K. L. Ronayne, H. Paulsen, A. Hofer, A. C. Dennis, J. A. Wolny, A. I. Chumakov, V. Schunemann, H. Winkler, H. Spiering, A. Bousseksou, P. Gutlich, A. X. Trautwein, J. J. McGarvey, *Phys Chem Chem Phys* **2006**, *8*, 4685-4693.

[13] a) S. Brüller, H.-W. Liang, U. I. Kramm, J. W. Krumpfer, X. Feng, K. Müllen, *J. Mater. Chem. A* **2015**, *3*, 23799–23808 ; b) Y. Zhu, B. Zhang, X. Liu, D. W. Wang, D. S. Su, *Angew. Chem. Int. Ed. Engl.* **2014**, *53*, 10673-10677.

[14] J. Blomquist, H. Lång, R. Larsson, A. Widelöv, *J. Chem. Soc. Faraday Trans.* **1992**, *88*, 2007-2011.

[15] U. I. Kramm, A. Zana, T. Vosch, S. Fiechter, M. Arenz, D. Schmeißer, *J. Solid State Electrochem.* **2016**, *20*, 969–981.

[16] a) E. L. Bominaar, X. Q. Ding, A. Gismelseed, E. Bill, H. Winkler, A. X. Trautwein, H. Nasri, J. Fischer, R. Weiss, *Inorganic Chemistry* **1992**, *31*, 1845-1854; b) J. Subramanian, *Electron Paramagnetic Resonance Spectroscopy of Porphyrins and Metalloporphyrins, Vol. 1*, Elsevier Sci Puplishing, Amstrerdam, **1975**.

[17] a) D. T. Petasis, M. P. Hendrich, in *Methods in Enzymology, Vol. 563*, Elsevier Scientific Publishing, **2015**, pp. 171-208; b) Y. Ohgo, Y. Chiba, D. Hashizume, H. Uekuas, T. Ozeki, M. Nakamura, *Chem. Commun.* **2006**, 1935–1937.

[18] U. I. Kramm, PhD thesis, Technischen Universität Berlin (Berlin), **2009**.

[19] a) B. Roldan Cuenya, L. K. Ono, J. R. Croy, K. Paredis, A. Kara, H. Heinrich, J. Zhao, E. E. Alp, A. T. DelaRiva, A. Datye, E. A. Stach, W. Keune, *Physical Review B*

2012, *86*; b) J. Marx, H. Huang, I. Faus, S. Rackwitz, J. A. Wolny, K. Schlage, R. Ulber, H. C. Wille, V. Schünemann, *Hyperfine Interactions* **2013**, *226*, 661-665.

[20] W. Zeng, A. Barabanschikov, N. Wang, Y. Lu, J. Zhao, W. Sturhahn, E. E. Alp, J. T. Sage, *Chem. Commun.* **2012**, *48*, 6340–6342.

[21] J. Li, Q. Penp, A. Barabanschikov, J. W. Pavlik, E. E. Alp, W. Sturhahn, J. Zhao, C. E. Schulz, J. T. Sage, W. R. Scheidt, *Chem. Eur. J.* **2011**, *17*, 11178 – 11185.

[22] B. K. Rai, S. M. Durbin, E. W. Prohofsky, J. T. Sage, G. R. A. Wyllie, W. R. Scheidt, W. Sturhahn, E. E. Alp, *Biophysical Journal* **2002**, *82*, 2951–2963.

[23] D. A. Scherson, C. A. Fierro, D. Tryk, S. L. Gupta, E. B. Yeager, J. Eldrige, R. W. Hoffman, *J. Electroanal. Chem.* **1985**, *184* 419-426.

[24] B. Roldan Cuenya, A. Naitabdi, J. Croy, W. Sturhahn, J. Y. Zhao, E. E. Alp, R. Meyer, D. Sudfeld, E. Schuster, W. Keune, *Physical Review B* **2007**, *76*.

[25] a) J. T. Sage, C. Paxson, G. R. A. Wyllie, W. Sturhahn, S. M. Durbin, P. M. Champion, E. E. Alp, W. R. Scheidt, *J. Phys.: Condens. Matter* **2001**, *13*; b) W. R. Scheidt, S. M. Durbin, J. T. Sage, *J Inorg Biochem* **2005**, *99*, 60-71.

Supporting Information:

Elucidating the structural composition of a Fe-N-C catalyst by nuclear and electron resonance techniques

S. Wagner [a,b], H. Auerbach [c], C.E. Tait [d], I. Martinaiou [a,e], C.N. Shyam Kumar [a,f], C. Kübel [a,f,g], I. Sergeev [h], H.C. Wille [h], J. Behrends [d], J.A. Wolny [c], V. Schünemann [c], U.I. Kramm *, [a, b, e]

Experimental part

Catalyst Preparation:

The investigated catalyst was prepared from iron porphyrin (FeTMPPCl, TriPorTech) supported on carbon precursor. In order to prepare the precursor, FeTMPPCl was dissolved in THF and then Ketjen Black 600 was added to the solution. After 1hour of continuous mixing, the solvent was evaporated with a rotary evaporator. The iron content in the precursor was 2.1 wt% Fe (95 % ^{57}Fe) on Ketjen Black 600. The precursor was subjected to a heat-treatment in inert gas atmosphere with a heating ramp of 300 °C h^{-1} to 600 °C and kept there for 30 min. 600 °C was selected as end temperature as previous results indicated that for this temperature the FeN_4 sites still remain intact [1]. After cooling down, the sample was transferred into 1 M HCl and acid leached. The suspension was placed for 1 hour in an ultrasonic bath and then remained in the acid overnight. After filtration and drying the catalyst was obtained as black powder.

^{57}Fe Mössbauer Spectroscopy:

Measurements at room temperature. Mössbauer measurements were performed with a RCPTM Mössbauer setup in transmission mode with a 3.7 GBq, ^{57}Co/Rh source and scintillation detector. 28 mg of the catalyst were prepared and measured under standard conditions within a velocity range of ± 6 mm s^{-1}. Afterwards, the isomer shifts were determined relative to α-Fe foil at 298 K. The collimators before and after the sample holder were adjust to 4 and 5, respectively. The Mössbauer spectrum at RT was analyzed using the program MossWin 4.0i [2].

LT-Mössbauer Spectroscopy.LT-Mössbauer spectra were recorded in horizontal transmission geometry using a constant acceleration spectrometer operated in conjunction with a 512-channel analyzer in the time-scale mode (WissEl GmbH). The detector consisted of a proportional counter filled with an argon-krypton-xenon mixture. The source contained ^{57}Co diffused in Rh with an activity of 1.6 GBq. The spectrometer was calibrated against α-Fe at room temperature (RT). For measurements at 77 K, samples were placed in a continuous flow cryostat (Optistat^{DN}, Oxford Instruments). Field-dependent conventional Mössbauer spectra at low temperatures were recorded with a closed-cycle cryostat from CRYO Industries of America, Inc. equipped with a superconducting magnet as described earlier [3]. Spectral data were transferred from the multi-channel analyzer to a PC for further analysis employing the public domain program Vinda running on an Excel 2003® platform [4] was used. The spectra were analyzed by least-squares fits using Lorentzian line shapes or in case of magnetically-split spectra by the spin Hamiltonian approximation, as described in the following [5]. For the fitting of LT Mössbauer spectra the experimental errors of the given isomer shifts δ_{iso}, quadrupole splittings ΔE_Q, and line widths Γ are on the order of ±0.02 mm s^{-1}, those of the magnetic hyperfine fields, B_{hf} are ± 1 T and of the asymmetry parameters, η are ± 0.2.

Spin-Hamiltonian Formalism in Mössbauer Spectroscopy. A paramagnetic iron with spin S in a ligand field is usually described by the electronic spin Hamiltonian (1) which can be used to calculate spin expectation values $<\vec{S}>$ [6]:

$$\hat{H}_S = D[\hat{S}_z^2 - S(S+1)/3] + E[\hat{S}_x^2 - \hat{S}_y^2] + \mu_B \vec{S} \cdot \vec{g} \cdot \vec{B} \quad (1)$$

where D is the zero field splitting, E/D the rhombicity parameter, μ_B the Bohr magneton. The ^{57}Fe nucleus senses the hyperfine field generated by the electronic spin. Mössbauer spectra were simulated using eq 1 together with the nuclear Hamiltonian:

$$\hat{H}_N = \frac{eQV_{zz}}{4I(2I-1)}[3\hat{I}_z^2 - I(I+1) + \eta(\hat{I}_x^2 - \hat{I}_y^2)] - g_N \mu_N \vec{I} \cdot \vec{B} + <\vec{S}> \cdot A \cdot \vec{I} \quad (2)$$

Here I denotes the spin quantum number of the nuclear states, Q the nuclear quadrupole moment, V_{zz} the z-component of the electric-field gradient (EFG) tensor, $\eta = (V_{xx} - V_{yy})/V_{zz}$ the asymmetry parameter of the efg, A the hyperfine coupling tensor which couples $<\vec{S}>$ to the nuclear spin $\vec{I}$ and g_N the nuclear g-factor.[7]

Nuclear inelastic scattering (NIS):

Nuclear inelastic scattering (also known as Nuclear Resonance Vibration Spectroscopy NRVS or Nuclear resonance vibrational spectroscopy NRIXS) was performed during the beamtime I-20160285 at the dynamics beamline P01 at PETRA III (DESY). The synchrotron worked in the 40 bunches filling mode with photon energy of 14.4 keV in combination with a high-resolution monochromator for ^{57}Fe. A catalyst powder package was prepared with the help of Kapton foil and mounted with a cooper sample holder in the closed cycle cryostat (6-800 K). The sample was cooled down to 46 ± 4 K. Four NIS scans were recorded with an avalanche photodiode (APD). Afterwards the spectra were summed up and the ^{57}Fe partial phonon density of states (pDOS) was calculated. Due to the homogenous distribution of particle orientation in the powder sample no orientation dependency of the projected pDOS has been observed.

DFT calculations:

The optimization of the structure models with different axial ligands, oxidation and spin-states of the iron centers for the initial Fe-N-C catalyst were performed with GAUSSIAN 09 [8] and were treated with density functional theory (DFT) using the functional B3LYP with the basis set CEP-31G.

X-band Electron paramagnetic resonance (EPR):

Samples for EPR measurements were prepared by filling 3.9 mm OD quartz tubes with 2.4 mg of the catalysts and flame-sealing the tubes after multiple cycles of pumping and purging with helium. X-band continuous wave EPR measurements

were performed on a home-built spectrometer consisting of a Bruker ER 041 MR microwave bridge with an ER 048 R microwave controller, an AEG electromagnet with a Bruker BH15 Hall effect field controller and using a Stanford Research SR810 lock-in amplifier with a Wangine WPA-120 modulation amplifier for field modulation and lock-in detection. The sample was placed inside an ER 4122 SHQE resonator and cooled to 5 K using an Oxford ESR910 helium flow cryostat with an ITC temperature controller. The spectra were acquired at a microwave frequency of 9.39 GHz and a microwave power of 62 µW with a 100 kHz modulation frequency and 0.5 mT modulation amplitude. A background correction was performed with the spectrum recorded for an empty EPR tube inside the resonator cavity. The Q-value of the resonator was determined from the mode picture for each measurement and used for the quantitative analysis and to compare relative intensities. Spin quantitation for high spin Fe(III) (S = 5/2) was performed by comparison to a reference sample of FeTMPPCl/CB (the precursor) with a known Fe(III) content of 1.62 wt% (determined by NAA). EPR spectral simulations were performed in Matlab with the EasySpin toolbox [9] for an effective $S' = 1/2$ spin system.

Microscopy:

Transmission electron microscopy (TEM) characterization was performed using an aberration (image) corrected Titan 80-300 (FEI Company) operated at 300 kV, equipped with a US1000 low-scan CCD camera (Gatan Inc.) for TEM imaging and a high-angle annular dark-field (HAADF) detector for STEM imaging. STEM imaging was performed with a camera length of 195 mm and a nominal spot size of 0.27 nm.

TEM sample were prepared by directly spreading the catalyst powder on holey carbon coated copper grids coated with an addition 3 nm carbon layer (Quantifoil).

Electrochemical Characterization:

Rotating Disc Electrode (RDE) measurements were performed with an ECi-200 potentiostat from Nordic Electrochemistry combined with an “EDI101” Rotating Disc Electrode setup from Radiometer. A three electrode setup was used with an Ag/AgCl/ 3 M KCl reference electrode and a Glassy Carbon (GC) rod as counter electrode. As working electrode, a GC disk (0.1963 cm^2) was used. The catalyst ink was prepared as follow; 5 mg catalyst powder were mixed with 223 µl of a 5 wt% Nafion solution (N/C = 0.48). The suspension was placed for 15 min in an ultrasonic bath, followed by dispersion with an ultrasonic finger and 5 min on a Vortexer. 5 µl of this ink was placed on the GC disk and left for drying at atmosphere (catalyst loading: 0.57 mg cm^{-2}). The electrochemical measurements were started in O_2 saturated electrolyte with two CV scans between 1.15 V and 0.0 V (vs. RHE) with 10 mV s^{-1} and 1500 rpm. Afterwards, the electrolyte was saturated with nitrogen and the catalyst was cycled 20 times with a sweep rate of 300 mV s^{-1} followed by a scan with 100 mV s^{-1} and a scan with 10 mV s^{-1}. Whereas the last-named scan is required for the correction of the capacity contribution from the scans in oxygen-saturated electrolyte. This protocol was used to have similar conditions in comparison to Herranz et al. [10].

HAADF-STEM

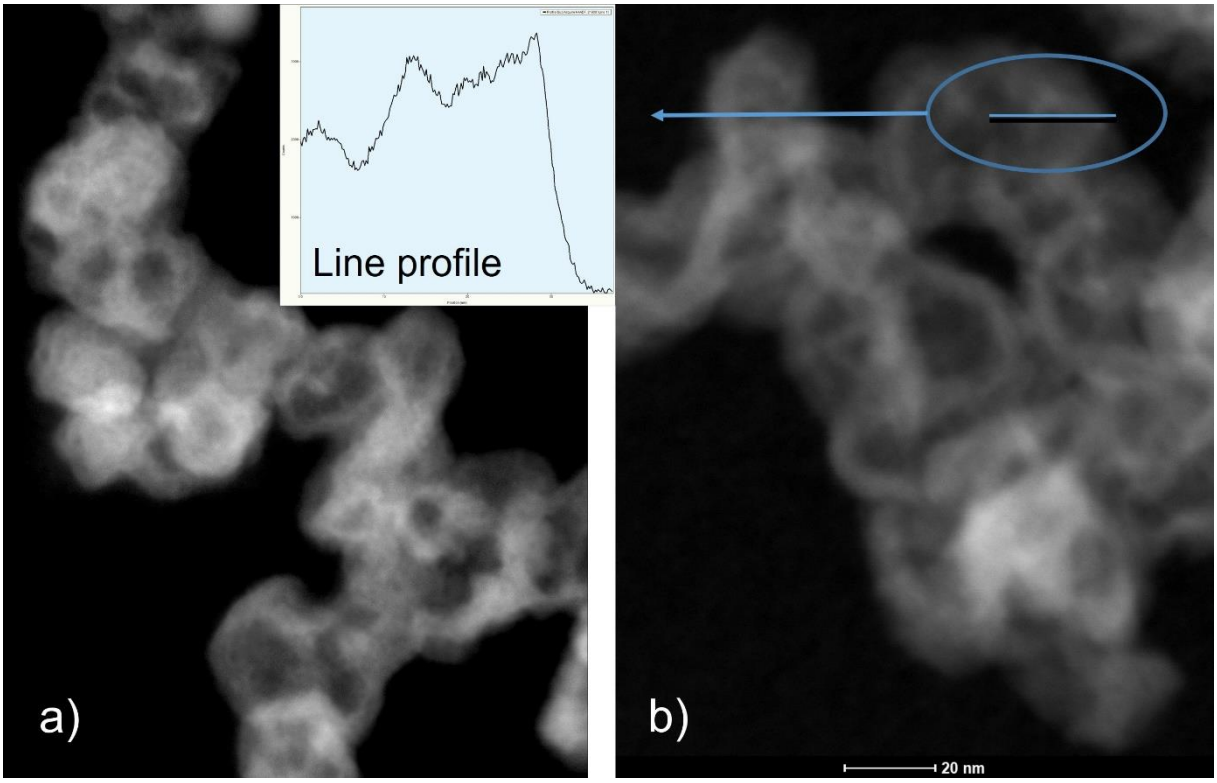

Figure S1. HAADF-STEM images of the catalyst including a line profile. The blue line in b) is added as guide for the eye.

EPR

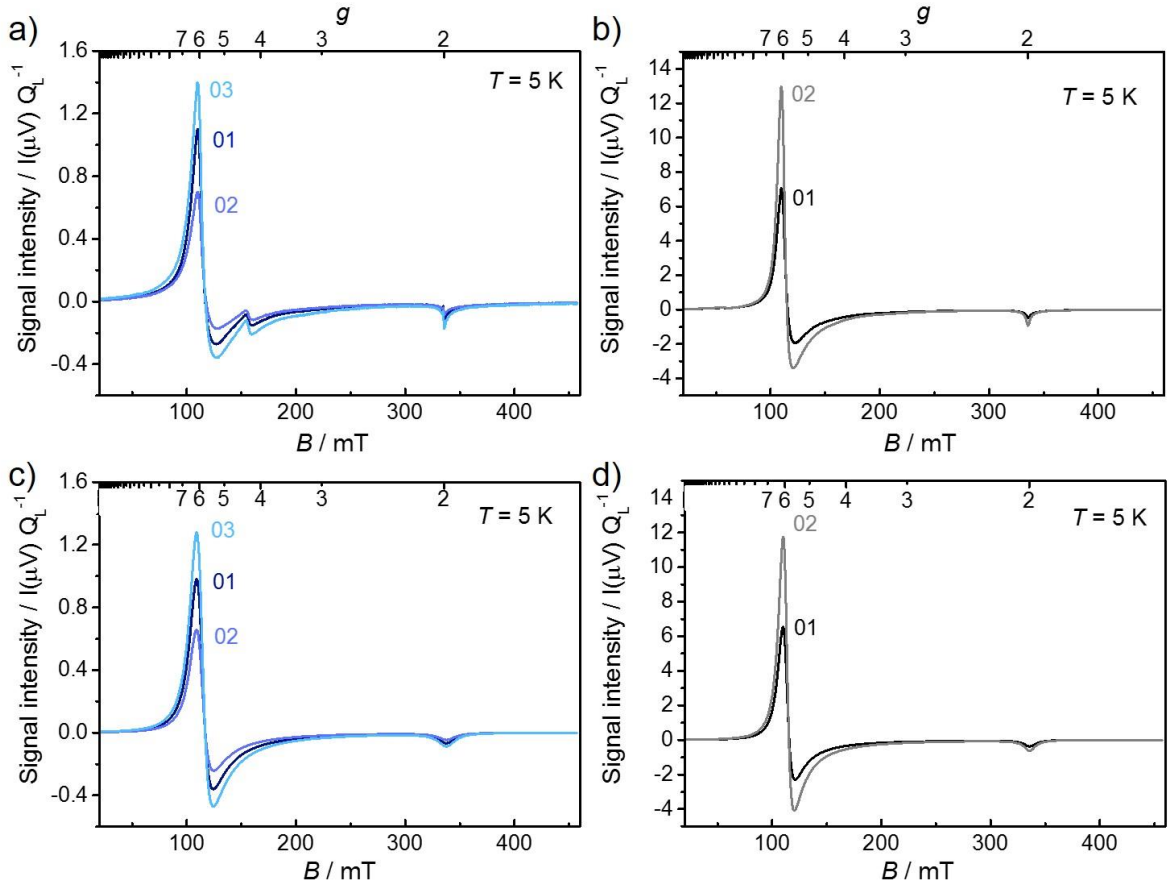

Figure S2. Experimental X-band EPR spectra of the catalyst powder (a) and the precursor (b) (ν_{mw} = 9.39 GHz, additional experimental details in text.) and EPR spectral simulations for (c) the catalyst powder (Simulation parameters: g_{eff} = [5.983 5.983 1.985] and Lorentzian line broadening of 10.6-10.9 mT) and (d) the precursor (Simulation parameters: g_{eff} = [5.982 5.983 1.9956] and Lorentzian line broadening of 7-7.7 mT for the precursor.).

Table S1.: Spectral areas and spin count determined from X-band EPR (ν_{mw}=9.39 GHz) on two precursor samples (FeTMPPCl/CB) with known Fe(III) content.

	weight / mg	wt % Fe(III)	N_{spins}	Area (exp.*)	Area (simul.*)
FeTMPPCl/CB 01	2.08	1.62	3.63E+17	4.83E-03	4.84E-03
FeTMPPCl/CB 02	2.69	1.62	4.69E+17	7.06E-03	7.61E-03

Table S2. Spectral areas, spin count and Fe(III) content determined from X-band EPR measurements on three samples of the catalyst by comparison with the precursor sample. Spin quantitation was performed based on a simulation of the high-spin Fe(III) EPR signal (values in parentheses are determined from the experimental data directly).

	weight / mg	Area* simul. (exp.)	N_{spins} Ref 01	N_{spins} Ref 02	wt % Fe(III) Ref 01	wt % Fe(III) Ref 02	wt % Fe(III)	St. Dev.
Cat 01	2.38	1.12E-03 (1.42E-03)	8.42E+16 (1.07E+17)	6.94E+16 (9.47E+16)	0.33 (0.42)	0.27 (0.37)		
Cat 02	2.42	7.84E-04 (1.14E-03)	5.87E+16 (8.57E+16)	4.83E+16 (7.59E+16)	0.23 (0.33)	0.19 (0.29)		
Cat 03	2.46	1.47E-03 (1.82E-03)	1.10E+17 (1.37E+17)	9.05E+16 (1.21E+17)	0.41 (0.52)	0.34 (0.46)	**0.29** (0.40)	**0.08** (0.08)

*The area corresponds to the double integral of the EPR spectrum divided by the Q-value determined for the corresponding measurement. All other measurement parameters were the same.

Electrochemical Characterization:

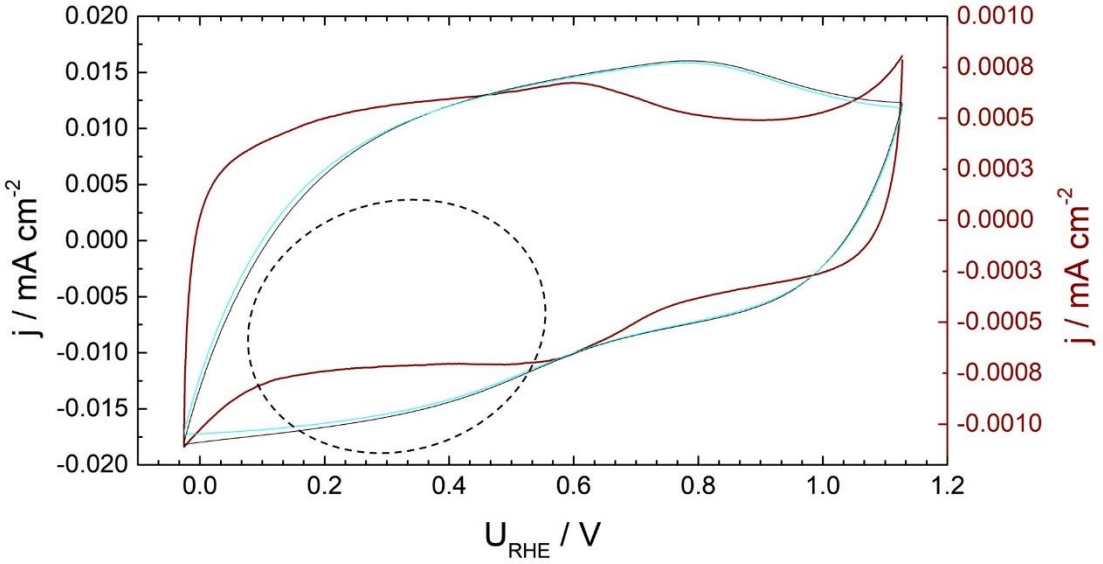

Figure S3. Cyclic voltammetry in N_2 saturated 0.1 M H_2SO_4: 1st scan (black curve) 20th scan (cyan) (both with 300 mV s^{-1} and CV sweep with 10 mV s^{-1} as used for subtraction for the RDE data.

In relation to literature, the electrochemical removal of iron, according to equation (3) is usually observed in the area indicated by the dashed cycle [11].

$$Fe^0 + H_2O \rightarrow FeO + 2\ H^+ + 2\ e^- \qquad (3)$$

The related oxidation peaks are usually only observed within the first cycle after contact with the electrolyte.

Supporting Information References

[1] U. I. Kramm, S. Fiechter, I. Abs-Wurmbach, I. Herrmann-Geppert, J. Radnik, P. Bogdanoff, *J. Electrochem. Soc.* **2011**, *158*, B69-B78.

[2] D. Z. Klencsár.

[3] A. Janoschka, G. Svenconis, V. Schünemann, *Journal of Physics: Conference Series International Conference on the Applications of the Mössbauer Effect (ICAME 2009)* **2010**, *217*.

[4] H. P. Gunnlaugsson, *Hyperfine Interact* **2016**, *237:79*.

[5] A. X. Trautwein, E. Bill, E. L. Bominaar, H. Winkler, in *Bioinorganic Chemistry. Structure and Bonding, Vol. 78*, Springer, Berlin, Heidelberg, **1991**.

[6] a) B. H. Huynh, T. A. Kent, in *Advances in Inorganic Biochemistry* (Eds.: G. L. Eichhorn, L. G. Marzilli), Elsevier, NewYork, Amsterdam, Oxford, **1984**; b) P. G. Debrunner, in *Iron Porphyrins Part 3* (Eds.: A. B. P. Lever, H. B. Gray), Wiley-VCH, **1989**, pp. 139–234; c) A. X. Trautwein, E. Bill, E. L. Bominaar, H. Winkler, *Struct. Bonding* **1991**, *78*, 1.

[7] E. Münck, J. L. Groves, T. A. Toumolillo, P. G. Debrunner, *Computer Physics Communications* **1973**, *5*, 225–238.

[8] G. 09, R. D.01, M. J. Frisch, *Gaussian Inc. Wallingford CT* **2009**.

[9] S. Stoll, A. Schweiger, *Journal of Magnetic Resonance* **2006**, *178*, 42-55.

[10] J. Herranz, F. Jaouen, M. Lefevre, U. I. Kramm, E. Proietti, J.-P. Dodelet, P. Bogdanoff, S. Fiechter, I. Abs-Wurmbach, P. Bertrand, T. Arruda, S. Mukerjee, *J. Phys. Chem. C* **2011**, *115*, 16087–16097.

[11] a) S. L. Gojkovic, S. Gupta, R. F. Savinell, *Journal of the Electrochemical Society* **1998**, *145*, 3493–3499; b) U. I. Kramm, Dr. rer. nat. thesis, Berlin, Technische Universität **2009**.